Simulations of Observed Lee Waves and Rotor Turbulence

HÁLFDÁN ÁGÚSTSSON

Institute for Meteorological Research, and University of Iceland, and Icelandic Meteorological Office, Reykjavík, Iceland

HARALDUR ÓLAFSSON

University of Iceland, and Icelandic Meteorological Office, Reykjavík, Iceland, and Bergen School of Meteorology, Geophysical Institute, University of Bergen, Bergen, Norway

(Manuscript received 25 June 2013, in final form 22 October 2013)

ABSTRACT

On 18 November 2008 a commercial aircraft encountered severe turbulence while flying in westerly flow along the southeastern coast of Iceland and descending from 2500 m down to the ground for a safe landing. Numerical simulations at horizontal resolutions of 9, 3, and 1 km are compared to the available observations. The simulations reproduce the situation, with an observed severe downslope windstorm at the ground as well as associated amplified lee waves and a rotor aloft, while climate data indicate that all observed westerly windstorms in the region are of the same type and occur in a similarly structured atmosphere. Strong shear turbulence is simulated at the interface of the lee wave and the rotor, as well as inside the rotor. The lee waves and the turbulence patterns are not stationary and as the upstream vertical wind shear increases, the lee wave becomes less steep, but the turbulence increases temporarily while the rotor circulation breaks down. From a forecasting perspective, this event could have been foreseen quite accurately, but not with the NWP tools that were in use for aviation forecasts, as their resolution was simply not adequate for resolving hazardous features of flow in and above complex terrain on the scale of this event. This event underlines the urgency of delivering products from finescale simulations over complex terrain to pilots and forecasters. Such products need to be developed taking into account the transient nature of the flows and the hazards.

1. Introduction

There is mounting evidence in the scientific literature that turbulence aloft over complex terrain may be successfully forecasted using finescale numerical simulations of the atmosphere. The verification of such simulations is, however, complicated by the lack of systematic three-dimensional observations aloft. Extensive observations of atmospheric turbulence are currently limited to large field experiments using specialized aircraft, such as over Greenland in the Fronts and Atlantic Storm Track Experiment (FASTEX; Doyle et al. 2005), the Greenland Flow Distortion Experiment (Renfrew et al. 2008), and the Terrain-Induced Rotor Experiment (T-REX) in the Sierra Nevada (Grubišić et al. 2008). These projects have gathered invaluable data, but they are expensive and unfortunately limited to intensive observations periods ranging from days to weeks, and may therefore miss extreme events. Apart from large experiments of this kind there are reported cases of turbulence aloft, for example, from aviation reports over Greenland and the Rocky Mountains in Colorado, as in Lilly (1978) where the turbulence was in fact observed by both commercial and research aircraft. Lane et al. (2009) studied a collection of turbulence events over Greenland in a systematic manner to identify flow regimes that contribute to unstable gravity waves and turbulence over Greenland. Ólafsson and Ágústsson (2009) focused on an international flight encounter with severe turbulence at the tropopause level in easterly flow over Greenland; an incident that could presumably have been avoided as finescale simulations reproduced the breaking waves and the turbulence that reached above the tropopause.

In fact, above and downwind of orography, gravity wave turbulence is primarily found at two height levels, as

Corresponding author address: Hálfdán Ágústsson, Institute for Meteorological Research, Orkugarði, Grensásvegi 9, 108 Reykjavík, Iceland.
E-mail: halfdana@gmail.com

DOI: 10.1175/MWR-D-13-00212.1

first was observed in the Sierra Wave Project in 1951–55 [rediscussed in Grubišić and Lewis (2004), see also references therein]. First, at upper levels (e.g., near the tropopause) clear-air turbulence may be encountered when vertically propagating gravity waves [see Durran (1990, 2003) for detailed reviews of gravity wave theory] overturn and break as a result of the strong and sudden change in atmospheric stability and even wind speed. Clear-air turbulence due to Kelvin–Helmholtz instability in regions of high wind shear (i.e., near the tropospheric jet) may also be encountered at the upper levels. Second, from ground level to a level well above the mountain tops there is a region where strong turbulence may be encountered, with the most intense turbulence often found in horizontally aligned rotors downstream of the mountains, as is the case in this study. Some of the first observations and a description of atmospheric rotors were made by Andrija Mohorovičić in 1888 in a study of orographic clouds during the Croatian Bora (Grubišić and Orlić 2007). In the first half of the twentieth century, atmospheric rotors were observed in the Sierra Wave Project [see Grubišić and Lewis (2004), and references therein] as well as in other projects such as the pioneering lee-wave study of Küttner (1938). In the latter half of the century there was considerably less effort dedicated to studies of rotors (Doyle and Durran 2004) but this has changed, partly because of the recent Sierra Rotors Project (e.g., Grubišić and Billings 2007) and the subsequent T-REX (Grubišić et al. 2008), which is the largest field campaign to date that is dedicated to observing rotors.

Hertenstein and Kuettner (2005) describe two possible types of rotors. The type-2 rotor is associated with hydraulic jumps and Hertenstein and Kuettner (2005) mention some of its documented observations. It supposedly has stronger and more intermittent turbulence than the type-1 rotor, which forms below amplified lee waves [first theory given by Scorer (1949)] and is characterized by reversed flow near or at the surface. As discussed in Doyle and Durran (2002), one of the first papers employing high-resolution numerical models in the study of rotors, lee waves facilitate the creation of rotors. The boundary layer flow separates from the surface at the lowest point of the wave because of the adverse pressure gradient set up by the wave, with larger waves in general leading to stronger rotors. The turbulent surface layer, which is characterized by strong forward wind shear and positive vorticity, contributes to the formation of the rotor when it is carried upward in the rising part of the wave. Idealized simulations with an atmospheric model suggest that friction is of paramount importance in the creation of rotors in real flows (see, e.g., Doyle and Durran 2002; Vosper 2004), while a secondary barrier downstream may cause constructive or destructive wave interference and affect rotor formation (Stiperski and Grubišić 2011). The contribution of a strong temperature inversion near the mountain top has been investigated by Vosper (2004) and has in general been found to have an impact on the formation of rotors, downslope windstorms, low-level turbulence, and hydraulic jumps. Idealized simulations of two- and three-dimensional flow over orography (Doyle and Durran 2007) indicate that small-scale and short-lived subrotors are created by shear instability on the rotor and lee-wave boundary. The subrotors are then swept along this boundary by the mean wind, and may be enhanced in flow over complex orography as opposed to idealized mountains, causing their turbulence kinetic energy to exceed that of the main rotor. That, together with their nonlocal and transient nature causes them to be possibly far more dangerous to aviation than the main rotors. These findings were verified in the first documented observations of subrotors during T-REX (Doyle et al. 2009).

This study reports on observations of severe turbulence in the lower troposphere in an aviation incident near the coast of southeast Iceland during the afternoon of 18 November 2008. The results presented here indicate that the turbulence was encountered in an atmospheric rotor, below a large amplitude lee wave. The observational data available during the turbulence event are described in the following section. In the subsequent section, a numerical climatology of similar events is analyzed. Section 4 describes the setup of the mesoscale numerical model used in section 5 to reproduce the atmospheric flow and the turbulence at varying horizontal resolutions. This is followed by discussions on the dynamics of the flow and an assessment is made of the potential for using high-resolution numerical simulations to improve aviation turbulence forecasts in complex orography. The summary and final remarks conclude the paper.

2. Observations during the event

According to the operational analysis from the European Centre for Medium-Range Weather Forecasts (ECMWF), at the time of the turbulence incident, there was a surface low to the north of Iceland and high pressure throughout the troposphere over the Atlantic Ocean south of Iceland (Fig. 1). The strong south–north-oriented pressure gradient gave rise to the strong westerly flow over Iceland, observed above the Keflavík upper-air station in southwest Iceland (Fig. 2). The strong westerly winds increase from $25\,\mathrm{m\,s^{-1}}$ below the top of an inversion at 900 hPa to nearly $45\,\mathrm{m\,s^{-1}}$ at midtropospheric levels, with weaker winds below the

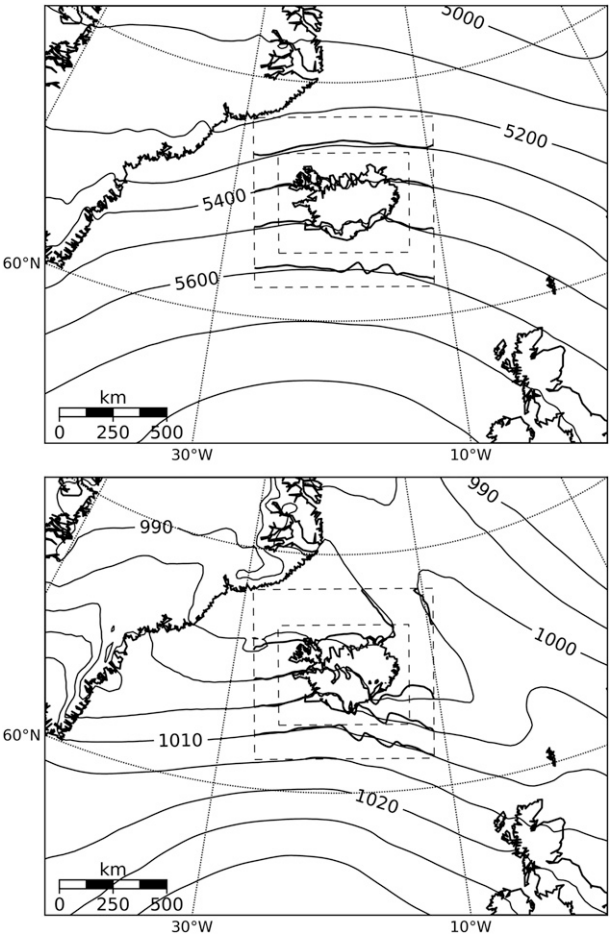

FIG. 1. Geopotential height at (top) 500 hPa in m and (bottom) mean sea level pressure in hPa at 1800 UTC 18 Nov 2008 (ECMWF operational analysis). Also shown are the same fields simulated at 9-km horizontal resolution, as well as the 9- and 3-km domain bounds (dashed lines).

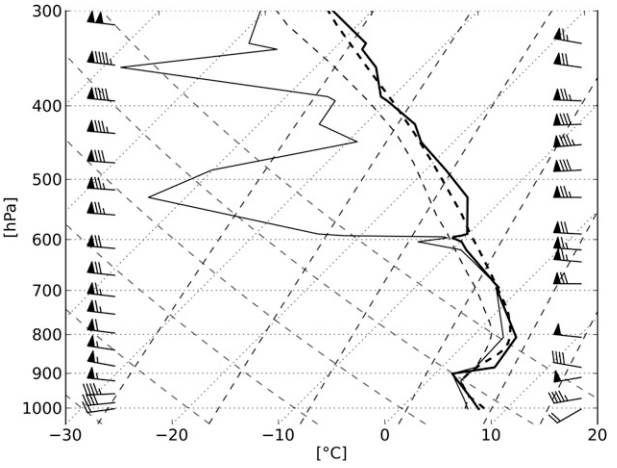

FIG. 2. Skew T–log$p$ diagram from the Keflavík upper-air station in southwest Iceland at 1200 UTC 18 Nov 2008. Shown are observed (solid lines) and simulated at 3-km resolution (dashed lines) temperature and dewpoint (°C) as well as wind barbs (2.5 m s^{-1} each half barb, observed to the right and simulated to the left) with temperature/dewpoint on the lower axis and height (hPa) on the vertical axis.

tropopause but stronger winds farther aloft. A backward trajectory analysis reveals the southern origin of the air mass (not shown). The relatively strong winds contribute to a well-mixed atmospheric boundary layer below 900 hPa.

The turbulence was encountered by a Cessna 406 Caravan II aircraft which is a fast dual-turboprop airplane that can carry nine passengers. It was on a scheduled flight for the Ernir airlines from Reykjavík in southwest Iceland to Höfn in Hornafjörður on the southeast coast (Fig. 3). The aircraft flew eastward along the south coast of Iceland at a cruising level of 3000 m (10 000 ft), with a strong tail wind. The plane first encountered the turbulence at the start of its descent at 2400 m (8000 ft) east of the ice covered Mt. Öræfajökull (2110 m) at 1635 UTC 18 November 2008 (the exact location is unclear). The severe, and even extreme, turbulence continued for 5–7 min while the aircraft descended to 900 m (3000 ft) and continued toward Höfn. The pilot tried to veer a few kilometers southward (i.e., away from the mountains), but the turbulence did not cease until the aircraft was close to landing at Höfn. A warning for this region [i.e., Significant Meteorological Information (SIGMET) (in this case a warning of moderate and severe clear-air turbulence)], was issued by Veðurstofa Íslands (VÍ; Icelandic Meteorological Office) after the incident [Airmen's Meteorological Information (AIRMETs) are not routinely issued in Iceland]. The pilots were experienced but had never encountered such strong and long periods of turbulence. They subjectively estimated that the acceleration was close to 2.5–3 g (where 1 g = 9.81 m s^{-2}) when the turbulence was strongest and they describe it as rapid but short up and down motion of the aircraft with approximately 45° changes in aircraft yaw. There were no clouds east of Mt. Öræfajökull at the time of the event, while there were, however, clouds upstream of the mountain and a cap cloud over the mountain from approximately 3700 to 6100 m (12 000–20 000 ft). The temperature near 3000 m (10 000 ft) was close to −3°C according to the pilots. It is not clear exactly where this temperature was observed but the sounding from Keflavík shows the same temperature at 3000 m. There were only minor personal injuries in the incident and the aircraft flew back to Reykjavík 1–2 h later, but this time it took a route over the Vatnajökull glacier with a strong head wind but without encountering turbulence.

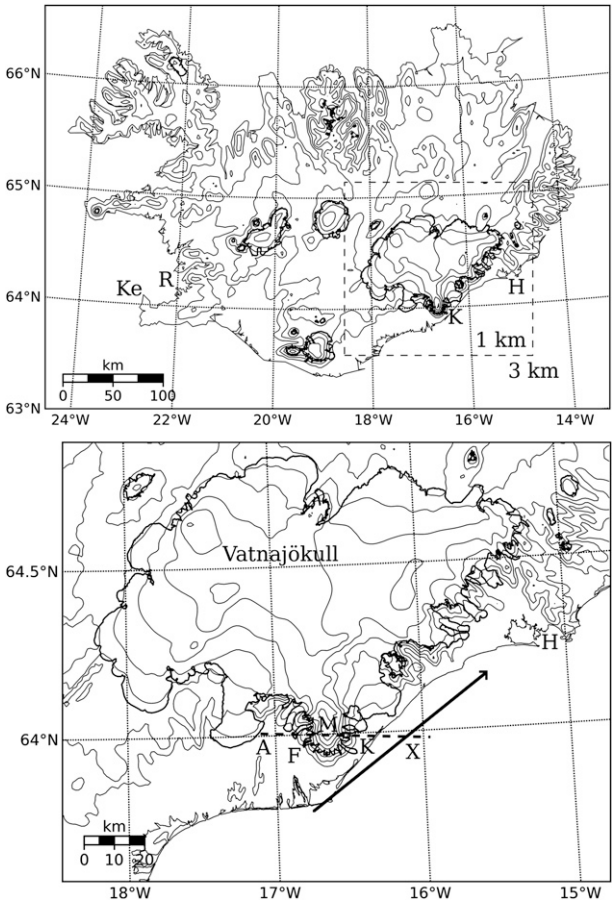

FIG. 3. Map of Iceland with terrain contours at 250-m intervals and model orography at a resolution of (top) 3 and (bottom) 1 km. Also shown are glacier outlines (bold), coastline, and the approximate track of the aircraft (arrow). The location where it first encounters the turbulence is denoted with a ×. The locations of Reykjavík (R), Höfn (H), Keflavík (Ke), Mt. Öræfajökull (M), Kvísker (K), Freysnes (F), section A, the Vatnajökull ice cap, and that of the 1-km numerical domain are also shown.

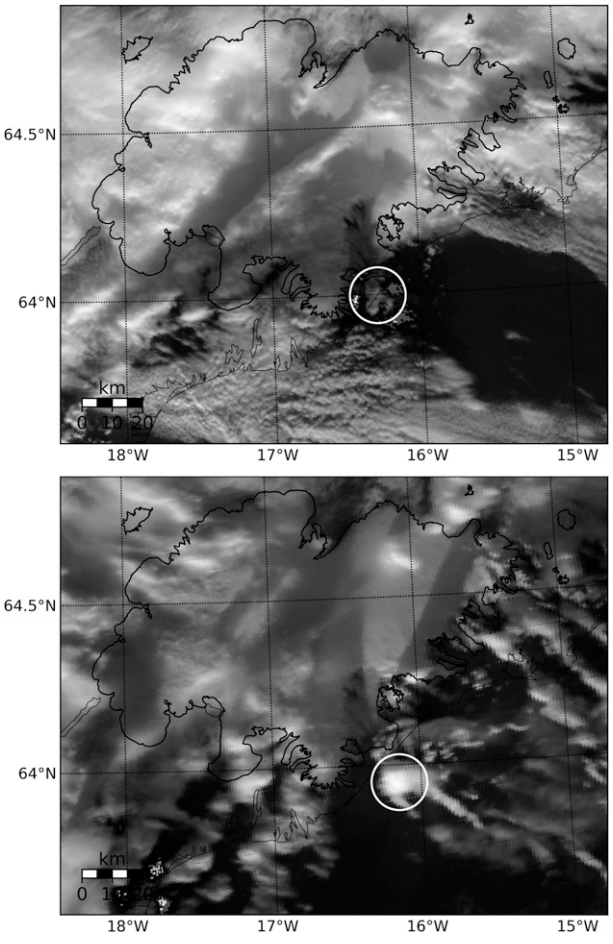

FIG. 4. MODIS images (courtesy of NASA) from the *Terra* satellite at (top) 1235 and (bottom) 1425 UTC 18 Nov 2008. Circles indicate the location of a possible rotor cloud.

Satellite imagery (clouds, Fig. 4) reveals clear features of wave activity in the atmospheric flow. The images compare well with the report of the pilots, taking into account the time difference between the imagery and the turbulence incident. Both available images reveal a cap cloud over Mt. Öræfajökull, but its height or vertical extent cannot be gleaned from the images. At 1235 UTC there are clear skies in a large wakelike region to the east of the mountain, while immediately east of the mountain (downwind), there is a broken cloud at or above mountain-top level that is reminiscent of a rotor cloud. At 1425 UTC, this cloud appears to have propagated a short distance downstream, and the skies are generally more cloudy with a banded pattern indicative of widespread gravity wave activity. The estimated path of the airplane will have taken it through or near the location of the possible rotor cloud in the second image. Note the indications of two distinct cloud types downstream of the mountain: the lighter-wave clouds and a darker, broken, cloud layer.

At approximately 1300 UTC a westerly (downslope) windstorm is first observed at the Kvísker weather station (location denoted in Fig. 3), with the 10-min wind speed at approximately 7 m above ground level increasing sharply from 5 to 30 m s^{-1} and gusting (3-s gust) to 40 m s^{-1}. At the same time there is significant warming and drying of the airflow, seen from the changes in 2-m temperature and dewpoint, equivalent to a decrease in relative humidity from 90% to 45% (Fig. 5). These observations are indicative of a gravity wave–induced windstorm where air from aloft is adiabatically warmed in an accelerated flow down the lee slopes of the mountain. A closer look at Fig. 5 shows that the winds, and in particular the wind gusts, start to pick up already before 1200 UTC, hinting to gravity wave activity aloft

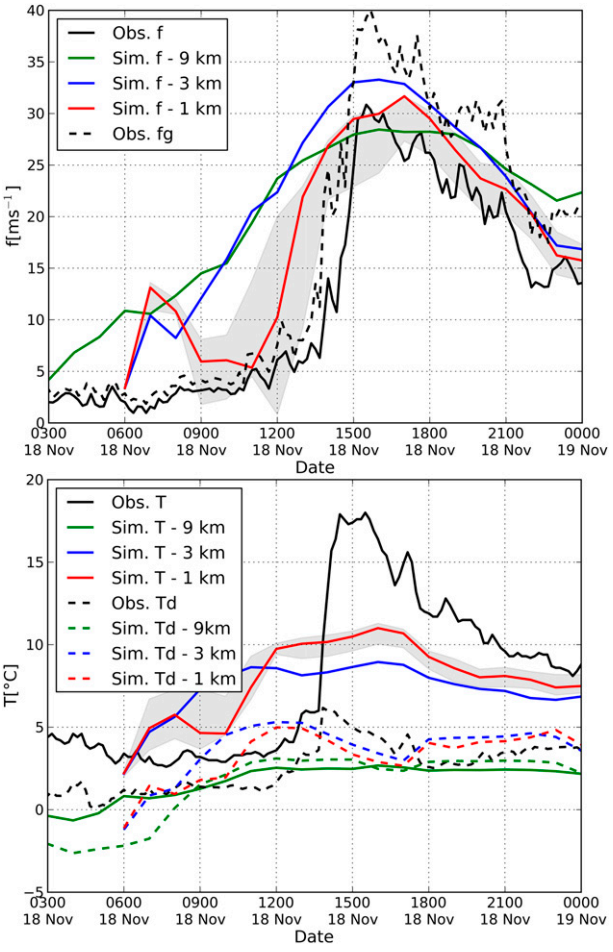

FIG. 5. (top) Observed and simulated surface wind speed at a resolution of 9, 3, and 1 km (C, M, and H runs), f (m s^{-1}), and observed wind gusts, f_g (m s^{-1}), as well as (bottom) observed and simulated temperature T and dewpoint T_d (°C) at the Kvísker automatic weather station on 18 Nov 2008. The gray shading shows values from a 3×3 km^2 area surrounding the closest grid point to the location of Kvísker in the 1-km grid.

at or before that time. It is in fact well-known from forecasters, local people, and mountaineers climbing Mt. Öræfajökull that during similar atmospheric conditions, there may be a windstorm of limited downslope extent on the upper slopes of the mountain, which may not be observed at the lowlands.

The automatic weather station at Kvísker (WMO No. 04886) is operated by Vegagerðin (the Public Roads Administration) and monitors a critical location on road No. 1 that is well known for severe local windstorms (Ágústsson and Ólafsson 2010) that disrupt traffic and even cause structural damage to the road itself. Observations from Kvísker and other automatic weather stations spread throughout Iceland are used for validating the atmospheric simulations presented in section 5. The

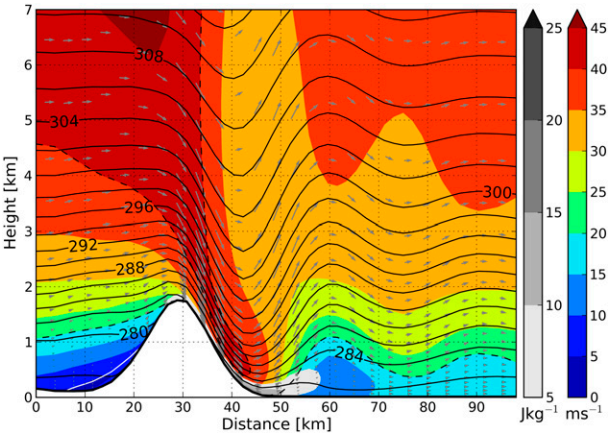

FIG. 6. Average wind speed (m s^{-1}), isentropes (K), turbulence kinetic energy (J kg^{-1}), and wind arrows along section A in the downscaled climate dataset (3-km resolution) during 30 westerly windstorms observed at Kvísker 2002–09. Dashed lines show wind speed contours at 20 and 40 m s^{-1}.

data from all the stations is stored and checked for systematic errors at VÍ.

3. Gravity wave climate

From 2002 to 2009, there were approximately 30 observations of westerly windstorms ($f_g > 35$ m s^{-1}) at Kvísker, all of which have been related to gravity wave activity aloft (Ágústsson and Ólafsson 2010). Here, in addition to simulating at high resolution the flow on the date of the turbulence incident, a four-dimensional dataset describing the state of the atmosphere in southeast Iceland during all westerly windstorms observed at Kvísker is prepared. In connection with the Reikningar á veðri (Simulations of weather; RÁV) project (Rögnvaldsson et al. 2011a), the ECMWF analysis was dynamically downscaled during 1994–2011 to a horizontal resolution of 3 km for Iceland. In fact, the dataset includes a large number of windstorms before operational observations at Kvísker as well as windstorms that are confined to the upper slopes of Mt. Öræfajökull and do not reach the site at Kvísker. The downscaling was performed using the Advanced Research Weather Research and Forecasting (WRF) Model (ARW, version 3.0.1; Skamarock et al. 2008) with a configuration equivalent to that used for the numerical simulations in this study. Gravity wave activity is in general well resolved in this region at a resolution of 3 km, including large amplitude lee waves associated with rotor formation; however, the resolution is not sufficient to resolve the rotors themselves.

A composite section (Fig. 6) across Mt. Öræfajökull reveals that the state of the atmosphere during observed westerly windstorms is on average characterized by

a deep upstream blocking, accelerated downslope flow, and a large-amplitude mountain wave immediately above Kvísker as well as waves farther downstream. An investigation of the individual windstorm events reveals that many of these events are associated with reversed surface flow below the first lee wave, indicative of a lee-wave rotor. During only one of the windstorms, does the vertical structure of the atmosphere deviate significantly from the mean state during the windstorms. In this event, the leeside flow resembles more a weak hydraulic jumplike feature than a train of lee waves (not shown).

There are unfortunately no systematic observations aloft available for validating the flow climate near Mt. Öræfajökull. However, satellite imagery of cloud cover and sea surface winds is available for four of the observed windstorm events and one recent event that was not observed at Kvísker (23 March 2011, Fig. 7). All the satellite images show signs of significant gravity wave activity aloft and there is a qualitative correlation with the structure of the vertical wind field at 3000 m from the dataset. All the events, except the one from 2011 when no windstorm was observed at Kvísker, have surface wind fields reminiscent of wave activity aloft, and there is good correlation between the Advanced Synthetic Aperture Radar (ASAR) image of 25 November 2008 and the corresponding surface wind field.

In summary, the climatological dataset as well as satellite imagery, indicate that during observed westerly windstorms, the atmospheric environment is characterized by significant gravity wave activity, including a train of lee waves as well as possibly rotors below the first wave in some of the events.

4. Setup of numerical simulations

The atmospheric flow on 18 November 2008 is simulated with the nonhydrostatic mesoscale ARW model (version 3.4.1; Skamarock et al. 2008). The model is initialized and forced at its boundaries with the ECMWF operational analysis (approximate resolution 25 km in 2008). The simulations are done at a resolution of 9, 3, and 1 km in order to investigate the dependance of the model performance on the horizontal resolution. A coarse resolution run (C) is done using only 9-km resolution, a medium-resolution run (M) is done using 9- and 3-km resolution, and finally a high-resolution run (H) is done at a resolution of 9, 3, and 1 km, with respectively 95×90, 205×157, and 190×175 grid points in the two-way nested domains (locations are shown in Figs. 1 and 3). Unless noted, the data from the high-resolution run (H) is presented. The simulations use 50 layers in the vertical, with higher resolution in the lower parts of the troposphere compared to farther aloft. The layers are terrain following at lower levels but flatten gradually toward the top of the model at 50 hPa. The model is run for 6 h before starting the nested domains at 3 and 1 km, which allows for approximately 10 h of spinup time before the time of interest. The boundary layer parameterization uses the Mellor–Yamada–Janjic (ETA) scheme (Mellor and Yamada 1982; Janjić 2001, 1994), which is frequently used for both research and operational simulations. This level-2.5 scheme uses a second-order moment closure for the turbulence and it is centered on the prognostic equation for the turbulence kinetic energy (TKE), which is consequently available as model output. Results from four small sensitivity tests are not presented here but they all gave similar and expected results. Namely, the case was also simulated using 40 layers in the vertical instead of 50, using the Global Forecast System (GFS) analysis, the ECMWF analysis on model levels, as well as using a modified version of the ETA scheme (Bao et al. 2008).

5. Simulations of the windstorms

The dynamics of the atmospheric flow on 18 November 2008 are investigated through numerical simulations. At the synoptic scale, the simulated mean sea level pressure and the height of the 500-hPa level at the coarsest resolution of 9 km compare well with the atmospheric analysis of the ECMWF, as depicted in Fig. 1 for the analysis time closest to the turbulence event. The large-scale fields are in general well captured, especially upstream of Iceland and away from the surface where the error in mean sea level pressure is less than 0.5 hPa and less than 10 m in the height of the 500-hPa level. The relatively large downstream disturbances to the south and to east of Iceland (1–2 hPa and up to 20 m) are a result of orographically disturbed flow. This is as expected because at a resolution of 9 km the orography is far better represented than at the much coarser resolution of the ECMWF analysis. Somewhat larger errors in pressure are found to the north of Iceland but here the pressure field is generally flat and the deviations are not expected to be relevant for the flow in southeast Iceland.

The upper-air observations from Keflavík in southwest Iceland (Fig. 2) are the only direct observations available aloft for verifying the upstream structure of the flow. At 1200 UTC, approximately 4 h before the turbulence incident, the model captures to a good extent the overall structure of the atmospheric profile above Keflavík (Fig. 2, no attempt is made to correct for the drift of the sonde). Finescale details in the temperature and wind profiles are generally not captured, while the overall vertical structure and hence atmospheric stability is correct. The most significant discrepancies are the slightly too shallow boundary layer with its top

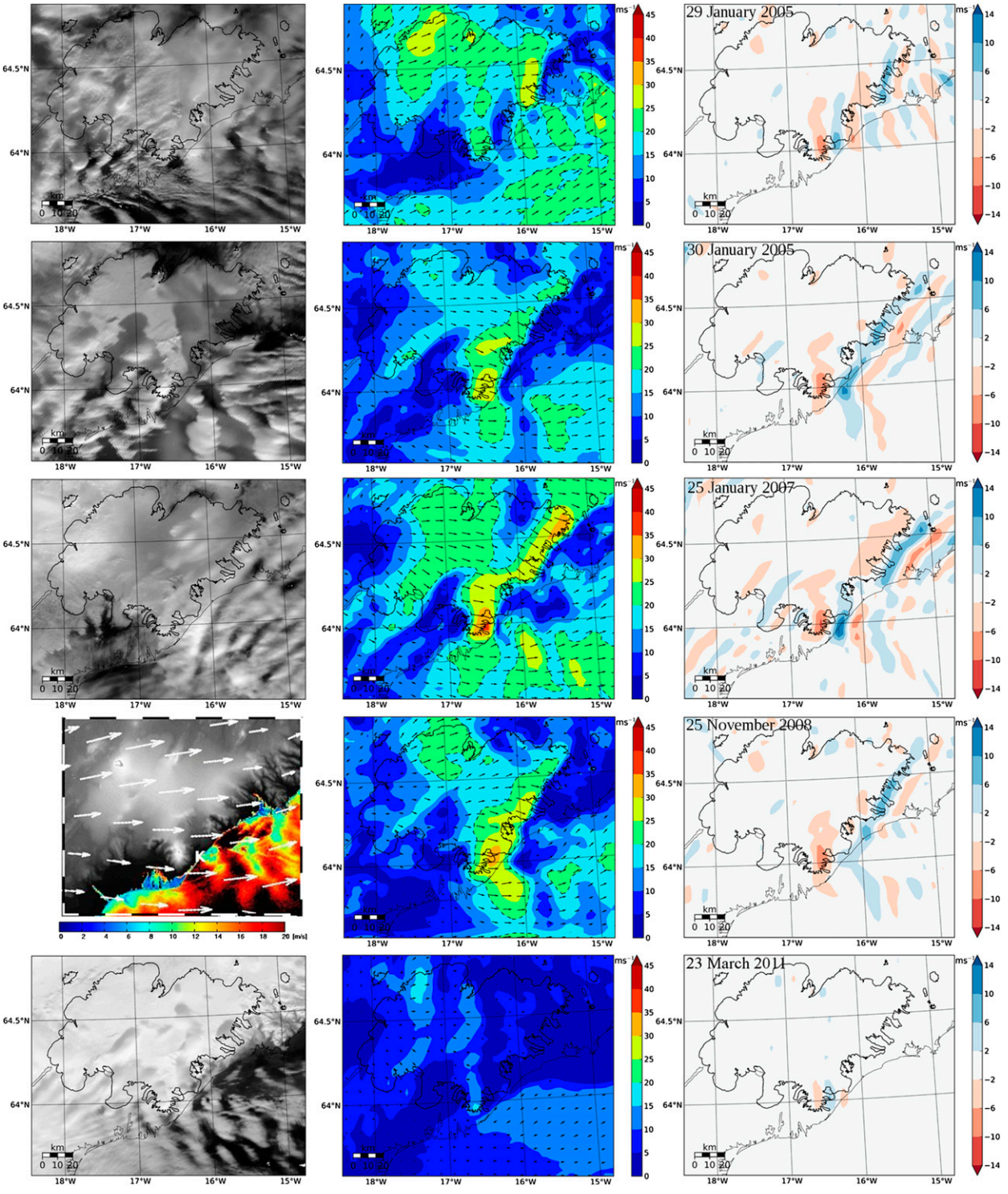

FIG. 7. (left) MODIS images (clouds, courtesy of NASA) and an ASAR image (sea surface winds, courtesy of the Nansen environmental and remote sensing center, Bergen, Norway). (middle) Surface wind speed ($m\,s^{-1}$) and wind vectors (20 and 40 $m\,s^{-1}$ contours dashed) and (right) vertical wind speed at 3000 m in the RÁV-dataset. (from top to bottom) Valid at (middle),(right) 1500 and (left) 1300 UTC 29 Jan 2005; (middle),(right) 1200 and (left) 1205 UTC 30 Jan 2005; (middle),(right) 1200 and (left) 1225 UTC 25 Jan 2007; (middle),(right) 1200 and (left) 1132 UTC 25 Nov 2008; and (middle),(right) 1200 and (left) 1250 UTC 23 Mar 2011.

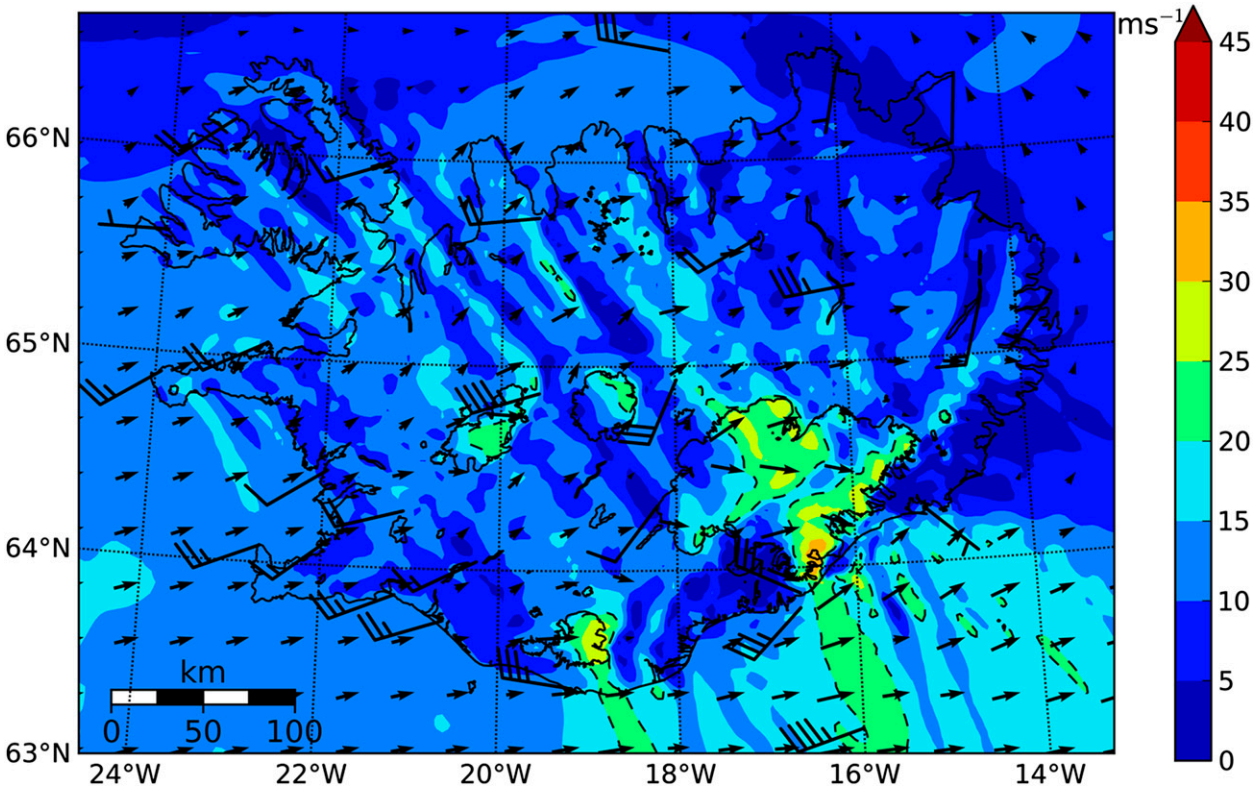

FIG. 8. Simulated surface wind speed (m s^{-1}) and wind vectors at a horizontal resolution of 3 km, as well as observed winds at automatic weather stations (2.5 m s^{-1} each half barb) at 1600 UTC 18 Nov 2008. The wind barb off the coast of southeast Iceland is inferred from satellite-borne scatterometer observations at a somewhat later time. Wind speed contours with a 5 m s^{-1} interval, with 20 and 40 m s^{-1} indicated by dashed lines. Glacier outlines are marked in bold.

at approximately 920 hPa instead of at 900 hPa, and the underestimation (2°–3°C) in the sharpness of the low-level inversion. Similar errors have previously been observed and are presumably a result of either too little vertical mixing by the boundary layer scheme or too small surface fluxes. The wind speed and the forward wind shear in the inversion are captured. In general the winds are overestimated by 1–3 m s^{-1}, but larger errors are found above the inversion and near the tropopause (5 m s^{-1} or even more). Humidity at upper-tropospheric levels is overestimated and its layering is not captured. There is a dry bias between approximately 850 and 630 hPa. Although the humidity near the boundary layer top is correct, the dry bias complicates a direct comparison between observed and simulated cloudiness. Somewhat similar errors in the layering of simulated humidity have previously been reported by Rögnvaldsson et al. (2007) for orographic flow in southwest Iceland, and were attributed to insufficient vertical resolution of the input data forcing the atmospheric model.

At the intermediate resolution of 3 km, the character of the simulated flow is that of flow strongly modified by orography (Fig. 8). The strongest winds are found along the edges and on the lee side of high mountains and glaciers, as well as off the southeast coast of Iceland where they have a wavelike pattern. There is a wakelike feature in the north. When compared to surface based observations (18 hourly) from the 27 locations depicted in Fig. 8, the mesoscale flow at a resolution of 3 km is in general correctly captured, as indicated by the statistics summarized in Fig. 9. The winds are on average underestimated by 0.3 m s^{-1} with a mean absolute error of 3 m s^{-1} or less at 20 locations. The mean error ranges between −6 and 4 m s^{-1}, with the errors in the range from −2 to 2 m s^{-1} at more than half of the stations. The greatest errors in wind speed and wind direction are in all cases found at locations where subgrid-scale orography is considered to be of importance, such as in the northwest of Iceland. At most of these locations, the observed wind speed and direction are within the range of the winds in a 6 × 6 km^2 region centered on the grid point closest to each location (not shown). Observed temperatures are captured with an absolute error of 2.5°C or less at all stations, and bias of less than 1°C at more than half of the stations. A large part of the error can be explained by errors in the representation of the

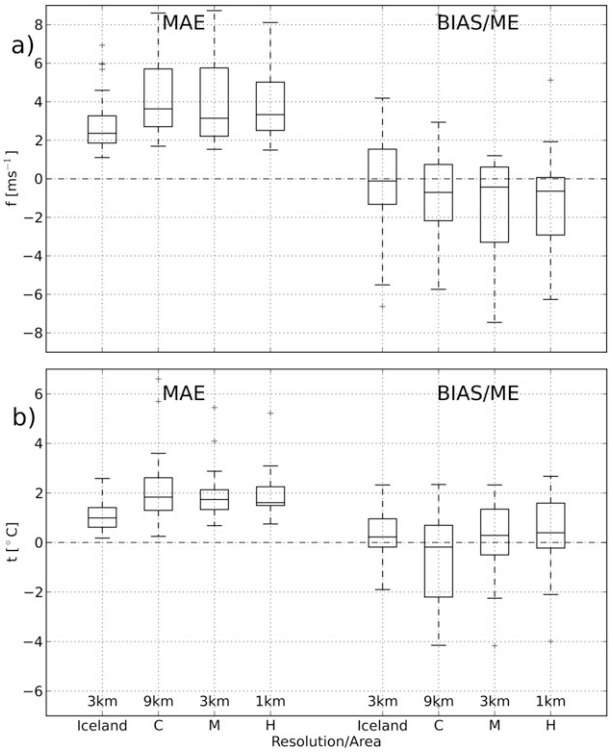

FIG. 9. Box-whisker plots showing mean absolute error (MAE) and mean error (ME/BIAS) for simulated (a) wind speed and (b) temperature. Data are from stations depicted in Fig. 8, in domain 1 at a horizontal resolution of 3 km covering all Iceland, as well for stations depicted in Fig. 10, for the C, M, and H runs in southeast Iceland. The median is given by the horizontal line inside the box that covers the 25% and 75% quartiles, while whiskers show the range of the data, excluding outliers.

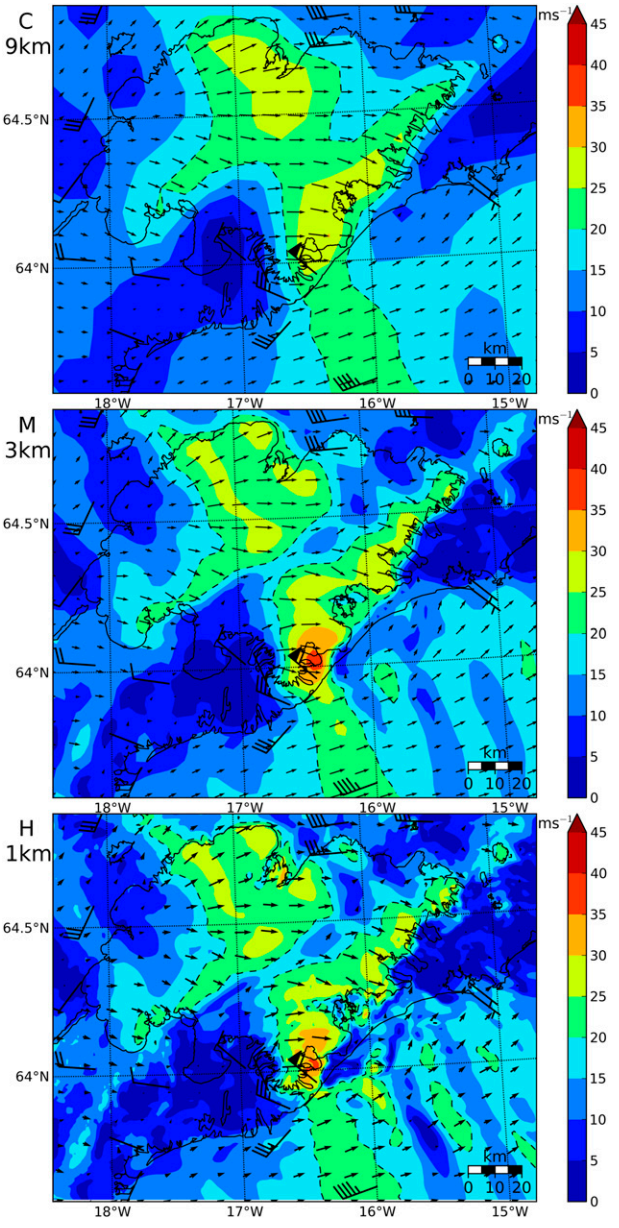

FIG. 10. Simulated wind speed (m s^{-1}) and wind vectors at a horizontal resolution of (top) 9, (middle) 3, and (bottom) 1 km from C, M, and H runs, respectively, as well as observed winds at automatic weather stations (2.5 m s^{-1} each half barb), at 1600 UTC 18 Nov 2008. The wind barb off the coast of southeast Iceland is inferred from satellite-borne scatterometer observations at a somewhat later time. Contours of 20 and 40 m s^{-1} are indicated by dashed lines, and glacier outlines are in bold.

actual station elevation in the model, which may be large in complex orography and are not accounted for here.

There is a dramatic increase in the detail of the simulated surface wind field in southeast Iceland when the horizontal resolution is increased from 9 to 3 km, for example, in the wave pattern at the surface on the lee side of Mt. Öræfajökull; a pattern that is not reproduced at a resolution of 9 km in the C run (Fig. 10). The increase in the complexity of the wind field is less pronounced when the resolution is further increased to 1 km, but the leeside winds become stronger. In general, there is improvement in the model performance, when the resolution is increased from 9 to 3 km, and to 1 km in the C, M, and H runs (e.g., which is summarized for wind and temperature in Fig. 9). However, there is only a limited number of automatic weather stations (16 in southeast Iceland), and while the spread of the mean and absolute errors for wind speed decrease with increased resolution, this increase in performance is not well reflected in the mean absolute error which has a median of almost 4 m s^{-1} in the C run and is close to 3.5 m s^{-1} in the M and H runs. Rather, the spatial structure not captured by the observational network and the time series of the winds should be investigated (e.g., at Kvísker; Fig. 5). At Kvísker, the winds are on average overestimated by 8.5, 8.7, and 5.1 m s^{-1} at a resolution of respectively 9, 3, and 1 km, which are the largest errors

for the observations shown in Figs. 9 and 10. The warming in the downslope flow, the weak flow before the start of the storm, the wind speed increase and the maximum wind speed during the storm are all best captured at a resolution of 1 km. The model performs reasonably well at 3 km but fails at a resolution of 9 km. The weak surface flow is well captured inside the relatively large-scale blocking on the upstream side of Mt. Öræfajökull (1–2 m s^{-1}), and the model performs quite well in the tip jet just south of Mt. Öræfajökull and at Höfn, the final destination of the airplane. At these two latter places, the deviations are well within the high spatial variability simulated in the surface wind speed and wind direction. Observed surface temperatures are on average better captured than observed winds, and there is a pronounced increase in the performance of the model when the resolution is increased from 9 to 3 km but little improvement is seen when the resolution is increased again to 1 km. The bias is 0°–2°C at more than half of the stations in the M and H runs, and the mean absolute error is near or less than 2°C for approximately 75% of the stations. The temporal behavior of both wind and temperature is best captured at 1 km, but there is on average a shift of 1–2 h in the time of start of the storm when compared to the observations. The temporal shift is smallest for the wind speed, slightly greater for the temperature, and greatest for the humidity. This shift in windstorm onset is greatest for the simulated flow at 9 km but it is to some extent seen at all resolutions, which indicates that it may in fact be related to slight errors in the boundary conditions. Previous studies of downslope windstorms in Iceland (Ágústsson and Ólafsson 2007) indicate that the error may also be connected to the horizontal extent of the downslope windstorm. In other words, it is possible that the timing of the onset of the downslope windstorm is correctly captured but that it was in reality limited to the upper slopes above Kvísker during the early hours of the windstorm and the simulation overestimated the speed with which the windstorm propagated downstream. This is supported by the satellite image from 1230 UTC (Fig. 4), which shows evidence of significant gravity wave activity before the onset of the observed windstorm at Kvísker (Fig. 5). In addition, an ASAR image (satellite born radar, not shown) shows a wavelike pattern in sea surface wind speed at 1144 UTC, approximately 10 km to the south and southeast of Mt. Öræfajökull (not shown).

The dry bias (Fig. 2) in the lower troposphere as well as the temporal and spatial variability in wave activity complicate the comparison of model output with observed clouds in the satellite imagery (Fig. 4). Nevertheless, the model simulates a cap cloud above Mt. Öræfajökull as observed by the pilots, a cloud above the lee slopes, and indications of wave like clouds downstream of the mountain (not shown). Simulated vertical wind speeds from the mountain-top level (i.e., 2000 m) show a pattern that resembles the observed cloud bands (cf. Figs. 4 and 11). The performance of the model appears somewhat better at 1400 UTC than at 1200 UTC, when the wave patterns are more pronounced and there are more clouds. From 1400 to 1600 UTC, at the time of the turbulence event, there is a slight downstream propagation and enhancement in the wave activity that can be inferred from the vertical wind field. The

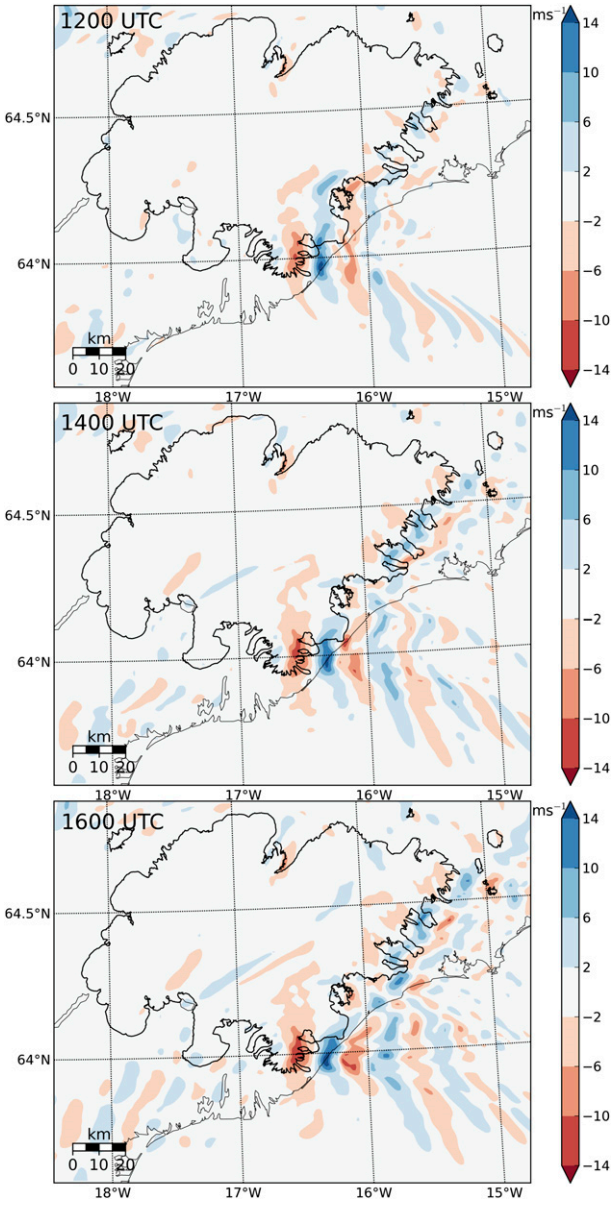

FIG. 11. Simulated vertical wind speed (m s^{-1}) at the 2000-m level, at a resolution of 1 km, at (top) 1200, (middle) 1400, and (bottom) 1600 UTC 18 Nov 2008.

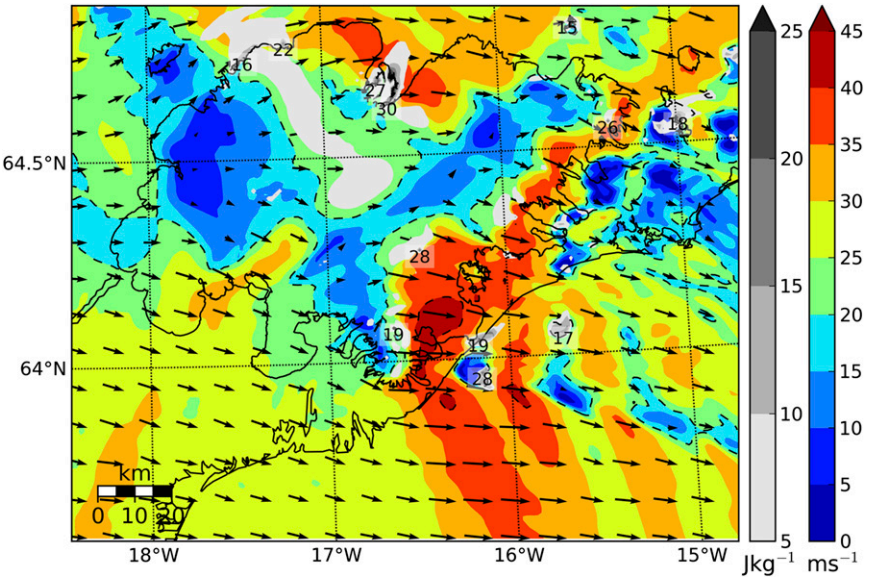

FIG. 12. Wind speed (m s^{-1}), wind arrows, and turbulence kinetic energy (J kg^{-1}), at a horizontal resolution of 1 km at 850 hPa at 1600 UTC 18 Nov 2008. Contours of 20 and 40 m s^{-1} are indicated by dashed lines and glaciers are marked with bold outlines.

simulated wavelength is slightly longer than that inferred from the satellite imagery (Fig. 4), but in this context the spatial and temporal variability in both simulated and observed wave activity should be considered. The path of the airplane would have taken it through or near regions with strong vertical winds, which are in fact found onward all the way to Höfn where the plane landed.

The winds at the 850-hPa level (Fig. 12) have a wavelike pattern in the lee of Mt. Öræfajökull, similar to that of the surface winds (Fig. 10) and the vertical winds at 2000 m (Fig. 11), correlating with the wavelike pattern in the cloud cover observed 1.5 h earlier at 1425 UTC (Fig. 4). At all resolutions, the maximum values of simulated TKE in the boundary layer are found in the surface flow above the leeside slopes of Mt. Öræfajökull. None or very weak turbulence is found east of the mountain at a resolution of 9 and 3 km. At a resolution of 1 km, the turbulence is strong and widespread (Figs. 12 and 13) with patches of large values of TKE and weak winds downwind of Mt. Öræfajökull, in the approximate path of the aircraft, as well as in complex orography along the eastern and northern border of Vatnajökull glacier. The turbulence strength was subjectively estimated by the pilots and can unfortunately not be compared directly with the simulated values of TKE. In spite of the spatial variability in the locations of the turbulence, caused by the nonstationarity of the flow, the locations correspond with those of the incident.

At resolutions of 1 and 3 km, several steep waves are simulated downstream of Mt. Öræfajökull (first wave shown in Figs. 14–15). Only a very small-amplitude wave is simulated at a resolution of 9 km in the C run, as may be expected from the much reduced height of the mountain forcing the wave compared to that in the H and M runs. The strongest winds are found above the slopes of the mountain in the descending part of the first wave at a resolution of 1 km. The largest values of TKE are found in regions of high wind shear at similar locations as well as below the rising part of the wave, also at a resolution of 1 km. A boundary layer separation occurs at the lowermost point of the wave, with far weaker and reversed surface flow below the rising part of the first wave. A horizontal rotor with clockwise rotation (positive vorticity, looking along the flow direction) is simulated underneath the first wave at a resolution of 1 km, with significant turbulence simulated at the rotor boundary. However, the wave pattern and the rotor are not stationary and as the waves become less steep, the rotor breaks down and the turbulence intensity varies greatly from 1600 to 1900 UTC (Fig. 15). There is decelerated and reversed flow inside a blocking on the upstream side of the mountain at resolutions of 3 and 1 km (M and H runs) but the blocking is weaker and there is no reversed flow simulated at 9 km (C run).

The extended turbulence reported by the pilots verifies the presence of extreme turbulence. Satellite imagery and surface-based observation of a downslope windstorm at Kvísker give on the other hand evidence for the rotor and the gravity wave activity. Overall, at a resolution of 1 km and to some degree at 3 km, the atmospheric flow can be considered to be adequately simulated.

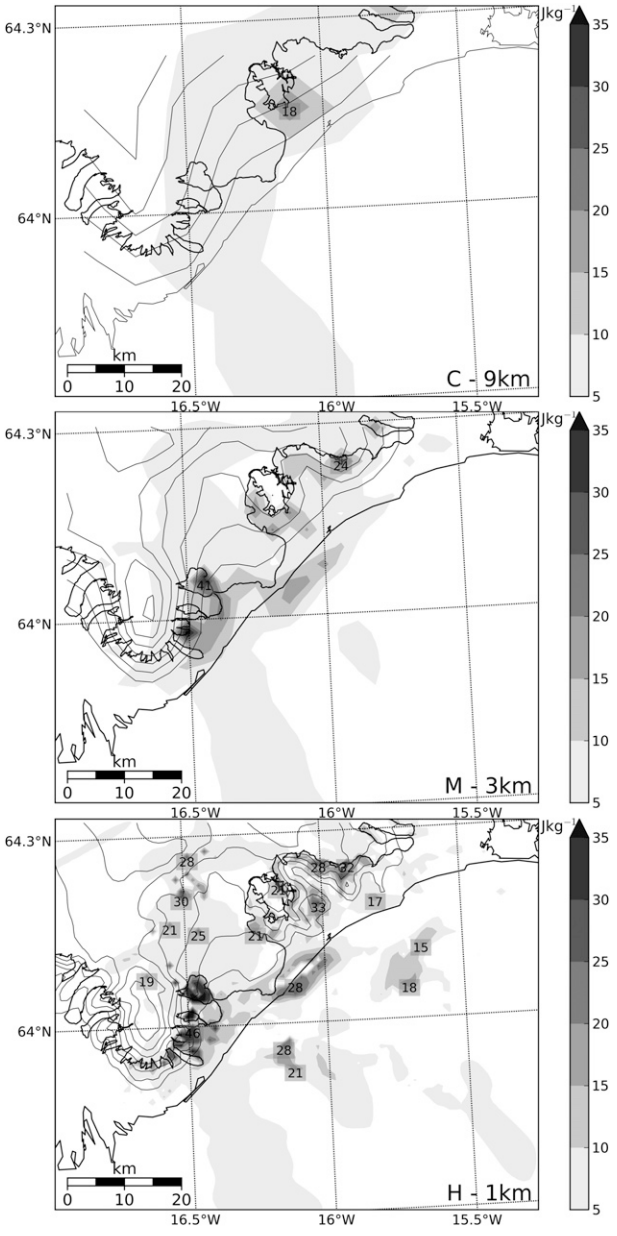

FIG. 13. Maximum boundary layer values (in each gridpoint column, extending from the surface and above the PBL) of turbulence kinetic energy (J kg^{-1}) at a horizontal resolution of (top) 9, (middle) 3, and (bottom) 1 km from the C, M, and H runs, respectively, at 1600 UTC 18 Nov 2008. Also shown are the coastline, glacier outlines (bold), and model orography with 250-m interval.

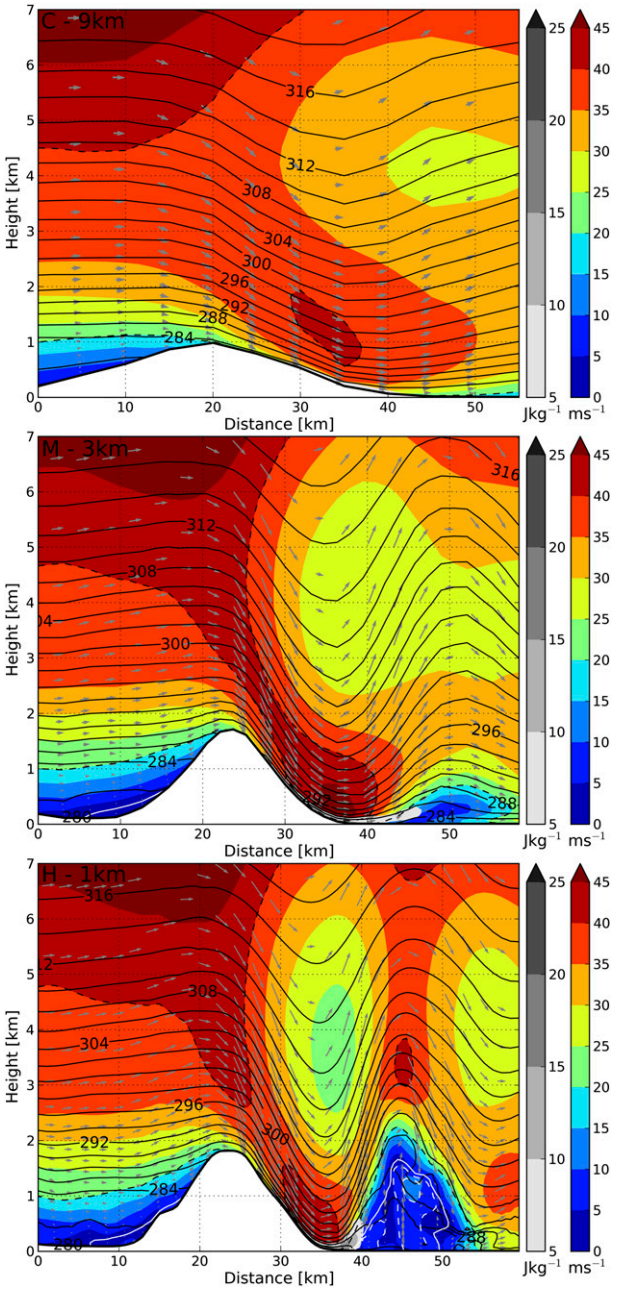

FIG. 14. Wind speed (m s^{-1}), wind vectors, turbulence kinetic energy (J kg^{-1}), and isentropes (K) at a horizontal resolution of (top) 9, (middle) 3, and (bottom) 1 km in the C, M, and H runs, respectively, along section A at 1600 UTC 18 Nov 2008. Also shown is the orography, dashed lines at 20 and 40 m s^{-1}, stagnant flow with a white line (0 m s^{-1}), and reversed flow with white dashed lines at 5 m s^{-1} intervals.

6. Discussion

a. The atmospheric flow

The atmospheric simulations reveal a large-amplitude lee wave and a rotor embedded in westerly flow off the coast of southeast Iceland. Figure 16 illustrates in a qualitative manner the complex three-dimensional structure of the wave activity with a secondary wave pattern resembling a bow wake. This parabolic-like structure resembles the wave pattern of linear theory (Smith 1980). This resemblance may be related to vertical variations in wind and stability being small above the mountain-top level. The turbulence incident occurred

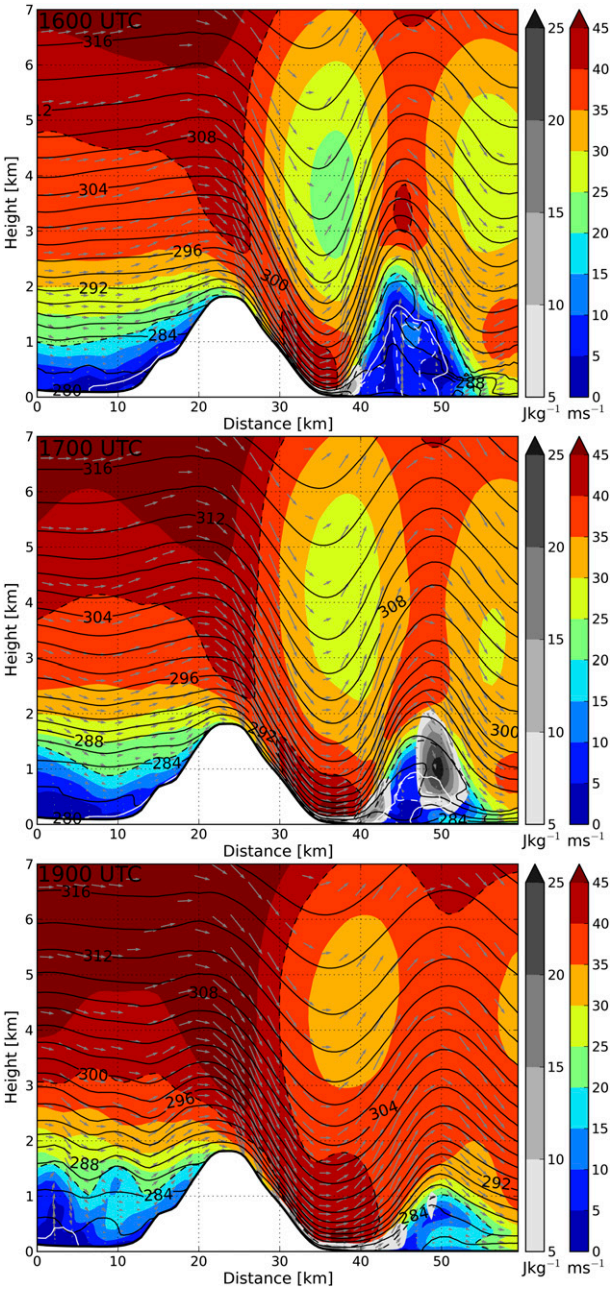

FIG. 15. Wind speed ($m\,s^{-1}$), wind vectors, turbulence kinetic energy ($J\,kg^{-1}$), and isentropes (K) at a horizontal resolution of 1 km along section A at (top) 1600, (middle) 1700, and (bottom) 1900 UTC 18 Nov 2008. Also shown is the orography, dashed lines at 20 and 40 $m\,s^{-1}$, stagnant flow with a white line (0 $m\,s^{-1}$), and reversed flow with white dashed lines at 5 $m\,s^{-1}$ intervals.

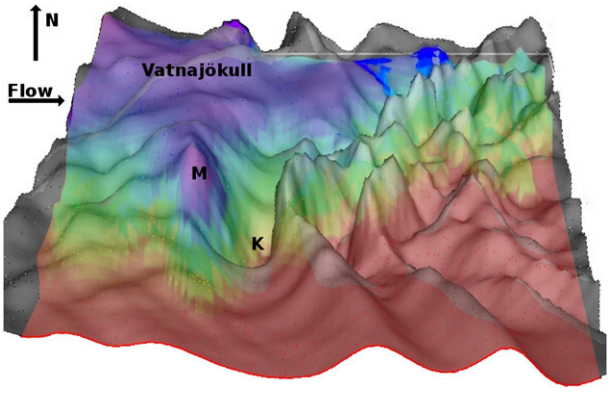

FIG. 16. Qualitative view of the 290-K isentrope surface in southeast Iceland at a resolution of 1 km at 1600 UTC 18 Nov 2008. Also shown are the direction of the flow, model orography height (increasing with height from red to purple), approximate locations of Vatnajökull glacier, Mt. Öræfajökull (M), and Kvísker (K).

when the aircraft flew through or near the upper part of the first lee wave and the rotor. This event is unique in the sense that previous incidents of the same kind in Iceland have not been documented as thoroughly and subsequently disseminated to the atmospheric research and forecasting community. The event is also quite unique in terms of the magnitude of vertical velocities that exceed those in previous studies (i.e., Sheridan and Vosper 2012).

The fast flow near the mountain-top level is necessary for the generation of the wave and conditions in the lower troposphere are favorable for the vertical propagation of the wave energy. In general, the surface conditions in the present case are favorable for formation of amplified waves and wave trains as the surfaces of both the glacier and the ocean are relatively smooth (e.g., Jiang et al. 2006; Smith et al. 2006). There is very little surface heating over the snow-free land and none at all over the ice and the sea, but surface heating is well known to have an impact on the lee waves (Smith and Skyllingstad 2009, 2011; Valkonen et al. 2010). An important issue in the context of this study is the location of the separation point. Not only is it important for the local weather forecast, but also for the drag force exerted by the mountain on the flow (e.g., Teixeira et al. 2013). Low roughness and surface heating move the separation point farther downstream (Doyle and Durran 2002). Here, surface heating by the November sun is very weak, but during other seasons it can be significant. If the glacier retreats, as is predicted in future climate, surface heating as well as surface roughness will increase, with the former tending to move the separation point farther downstream and the latter tending to move it upstream.

There is a further contribution to the generation of the wave and the rotor by the strong inversion near the mountain-top level and the forward wind shear through it, capping the relatively shallow but well mixed boundary layer (Vosper 2004; Hertenstein and Kuettner 2005). Weak forward wind shear is observed and simulated at the upstream location of Keflavík, but no observed profiles are available at locations closer to Mt. Öræfajökull.

The simulated gravity waves are not stationary and there is significant development in the rotor and turbulence during the windstorm. The upstream wind speed and the vertical wind shear increase with time. The separation point moves downstream and the rotor turbulence increases, while the amplitude of the lee wave decreases (Figs. 15 and 16). This is in agreement with the well-known linear connection between wind speed and horizontal wavelength. Presumably, the modifications in the lee flow are mainly related to the changes in the upstream winds while surface heating is of little importance as previously mentioned. The leeside development appears to be related to changes in the upstream flow, but this connection may be complicated and highly nonlinear as is discussed in Nance and Durran (1997, 1998) and model dependent (Doyle et al. 2011). Even with the relatively long distances to significant upstream orography, wave interference may be relevant (Grubišić and Stiperski 2009; Stiperski and Grubišić 2011). Furthermore, studies of ensembles of simulations of downslope windstorms show a significant sensitivity to small-scale features in the initial conditions (Reinecke and Durran 2009), but it is not clear what aspects of the synoptic-scale flow have the greatest impact on the predictability of the windstorms. Gohm et al. (2008) found a strong dependence of the downstream propagation of lee-wave rotors and hydraulic jumps on the turbulence parameterization. They attributed the too-early onset of the bora to be due to insufficient mixing in the boundary layer. The situation here is reversed, that is, the windstorm onset is delayed at Kvísker, which according to Gohm et al. (2008) might be a result of too much mixing by the ETA PBL scheme. This is in fact plausible but remains to be investigated.

Locally, the highest values of subgrid TKE are found in the rotor and in a shallow layer in the descending flow over the lee slopes of the mountain, and are in excess of 40 J kg^{-1} in the 3- and 1-km meshes at 1600 UTC. This turbulence and the embedded positive vorticity due to forward wind shear near the surface are carried upward at the separation point and into the rotor circulation [as discussed in Doyle and Durran (2002)], where the maximum TKE values are on the order of 30 J kg^{-1}. The observed gusts (f_g = 40 m s^{-1}) at Kvísker are a manifestation of the turbulence over the lee slope, while the gust factor ($G = f_g/f$) of 1.3–1.5 is not as high as might be expected from the proximity to Mt. Öræfajökull (Ágústsson and Ólafsson 2004). It might possibly be higher had the accelerated flow been a result of a hydraulic jump aloft instead of a lee wave, and hence possibly more turbulent. The total vertically integrated TKE is greatest in the lee-wave rotor and is nearly 10 times as great as the maximum point value at the surface (i.e., 300 J kg^{-1} at a resolution of 1 km at 1600 UTC; not shown). At a resolution of 3 km, the values of the TKE are

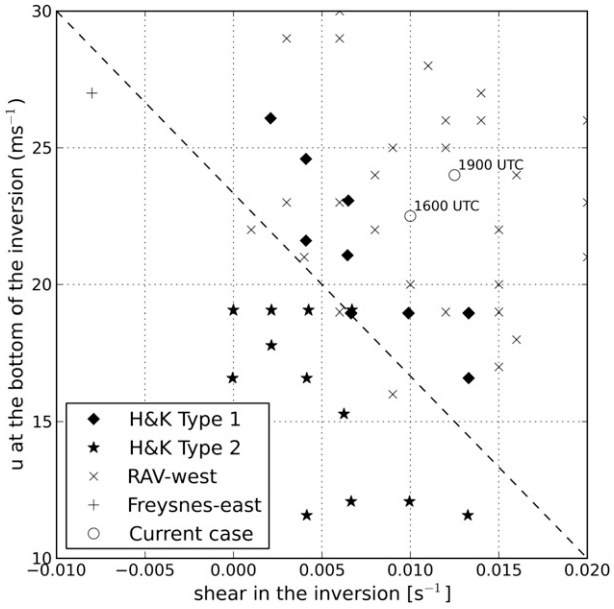

FIG. 17. The upstream vertical structure of temperature and wind at Mt. Öræfajökull for all westerly windstorms from the climate dataset (RÁV project) [crisscross (×)], the Freysnes easterly windstorm [plus symbol (+)], as well as the rotor in the current case [open circle (o)] superimposed on the rotor diagram in Hertenstein and Kuettner (2005, their Fig. 16), with initial flow velocity at bottom of the inversion vs initial shear through the inversion in idealized simulations.

50%–75% of the values at 1-km resolution and at a resolution of 9 km, the values of the TKE are down to about 10%–20% of the values at 1 km. In spite of the improvement in the simulations of the flow, it may be argued that a part of the subgrid TKE at a resolution of 1 km is in fact also explicitly resolved by the atmospheric model and the boundary layer scheme (Deng and Stauffer 2006; Wyngaard 2004). The experience with this particular setup of the atmospheric model (ARW) is that this is not the case for resolutions near 1 km, while it is, however, not clear what happens at higher resolutions (e.g., Horvath et al. 2012).

The lee-wave rotor is of type 1 as classified by Hertenstein and Kuettner (2005). This is in agreement with the wind and temperature profiles in the boundary layer and through the inversion (Fig. 17), as seen when the current case is superimposed on the rotor diagram in Hertenstein and Kuettner (2005, their Fig. 16). The maximum TKE values in the simulated rotor in the current study are 2–3 times greater than in the idealized study of Hertenstein and Kuettner (2005), where the maximum TKE values were near 13 J kg^{-1}. This is at least partly a result of the differences in the topography and structure of the real flow presented here and the setup of the idealized study of Hertenstein and Kuettner (2005). The simulated TKE values in the current study are similar to observed values discussed in Smith (1987) and (Gohm

et al. 2008). From Fig. 17, the present case is well within the type-1 region and substantial changes of the flow are needed to enter the type-2 hydraulic jumplike region. With a similar wind shear, the winds at the inversion would have to decrease by 5–10 $m s^{-1}$, while with a weaker positive wind shear, or even better, a negative wind shear, the needed wind speed decrease is more modest. The turbulence in rotors of type 2 appears to be more intense and transient than in rotors of type 1 (Hertenstein and Kuettner 2005) and it may be postulated that had the aircraft flown through a type-2 rotor it could have had more serious consequences than was the case here. Although small variations of the flow are not likely to make the current windstorm enter the type-2 rotor regime, such flow regimes may, however, occur in the region, but preferably in a type E (extended) downslope windstorm in northerly flow, as described in Ágústsson and Ólafsson (2010). Although the observed Kvísker westerly windstorms of type S (short) are gravity wave generated, it does not exclude the possibility of westerly windstorms associated with hydraulic jumps, which may develop from overturning amplified lee waves as suggested by Vosper (2004). In fact, a few of the cases from the climatological dataset are located only a small distance into the regime of rotors of type 2, in the transition zone between the two rotor types (Fig. 17). A manual inspection of these cases does, however, confirm that they feature a type-1 wavelike flow, at least during the periods inspected. The previously documented and well-known easterly Freysnes windstorms occurring at the western edge of Mt. Öræfajökull (cf. Fig. 3), are a result of gravity wave breaking aloft and in that sense that they resemble a hydraulic jump (Ólafsson and Ágústsson 2007; Rögnvaldsson et al. 2011b). The Freysnes windstorm is indeed located inside the type-2 region in Fig. 17, although the wind speed at the inversion is far greater than in the idealized cases of Hertenstein and Kuettner (2005) and no rotor of type 2 was reproduced at 1-km resolution in the numerical simulations of Ólafsson and Ágústsson (2007) and Rögnvaldsson et al. (2011b). It is of interest in this context that Gohm et al. (2008) found evidence of lee-wave rotors alongside hydraulic jumps at neighboring locations in bora flow across the Dinaric Alps. The leeside variability in flow structure was mainly attributed to differences in the height of the topographic barrier, leading to local variations in the governing flow parameters. Similar features may at times be a part of the Mt. Öræfajökull flow.

b. *The forecasting perspective*

It is indeed known that improvements in flow details are obtained by increasing the numerical resolution in the vicinity of complex terrain. However, here it is shown that a major flow regime shift occurs in the numerical simulations when moving from horizontal resolution of 9 to 3 km. This shift corresponds to a change from moderate to extreme weather conditions for air traffic and conditions at the surface of the earth. Needless to say, a similar shift may occur at different resolutions in other parts of the world and in different weather situations. In this case, the necessary horizontal resolution needed to successfully simulate the event is 5–10 times greater than the resolution of the operational numerical models, on which many NWP products for aviation are based. This dependence on resolution is not only valid at low-tropospheric levels, but at levels of international air traffic as shown by Doyle et al. (2005) and Ólafsson and Ágústsson (2009). Furthermore, amplification of gravity waves, overturning, and breaking, as well as trapped lee waves are nonhydrostatic phenomena that cannot be expected to be correctly represented in many of the aforementioned coarse resolution and hydrostatic numerical models.

This study is partly motivated by results from the Háupplausnar reikningar til almennrar spágerðar (high-resolution atmospheric simulations; HRAS) system, which at the time of the incident was the only high-resolution (9 and 3 km) operational forecasting system in use in Iceland (Ólafsson et al. 2006). It correctly simulated the wave activity and the observed downslope windstorm at the surface at Kvísker at a resolution of 3 km, with the nonhydrostatic ARW model and the fifth-generation Pennsylvania State University–National Center for Atmospheric Research (PSU–NCAR) Mesoscale Model (MM5; Grell et al. 1994), forced by operational GFS and ECMWF forecasts, respectively. It appears that these high-resolution numerical simulations were unfortunately not taken into account in the forecasting process, which was presumably based on other available and coarser grid hydrostatic models. Consequently, no warning (SIGMET) was issued for the region until after the turbulence incident.

Although the full four-dimensional structure of the atmosphere is of course simulated by operational numerical weather prediction models, there is at the moment only a limited dissemination of the finescale elements of the flow aloft, both over Iceland as well as over many other regions of the world. This study indicates that more systematic dissemination in four dimensions of high-resolution simulations of the atmosphere will definitely be of substantial value for pilots and forecasters in or near mountainous regions. This accounts not only for basic parameters such as wind and temperature, but also for secondary parameters like turbulence and icing. Although the numerical simulations are essential for developing systems for forecasting these

secondary parameters, observations, and in particular satellite imagery, may provide additional useful information for such systems, as shown by Feltz et al. (2009). In short, the present study leads to the following recommendations for the forecasting communities, as well as for researchers analyzing or developing weather warning systems:

1) Numerical simulations at high spatial resolutions can be a valuable addition to the tools available for forecasting severe weather in the vicinity of complex terrain. Interpolation from coarse-resolution simulations may lead to large errors, even if the mountains are to some extent represented.
2) Because of the often transient nature of perturbations induced by mountains and the associated difficulty in simulating them accurately, weather warning systems could benefit from an evaluation of the variability (and the predictability) of the simulated flow in time, as well as in space. The importance of this is in line with some previous studies (e.g., Reinecke and Durran 2009).
3) Ground observations of weak winds at locations where downslope windstorms may be expected, are not a reliable indicator of absence of waves and turbulence aloft.

7. Summary and conclusions

This paper describes a severe turbulence event in the lee of Mt. Öræfajökull in southeast Iceland, documented by a small passenger airplane. The turbulence, amplified lee waves and a horizontal rotor, as well as an observed gravity wave generated downslope windstorm, are realistically simulated by a numerical model. We have a type-1 rotor as classified by Hertenstein and Kuettner (2005), which is in agreement with the vertical profile of wind and temperature. There is strong shear turbulence in the lee wave, at the wave and rotor interface, as well as inside the rotor. The waves are not stationary and the rotor turbulence increases while the lee-wave amplitude decreases in the late afternoon.

Observations of severe turbulence aloft in a situation of this kind are relatively rare but when they occur they provide important occasions to verify the performance of the atmospheric models. These observations also provide valuable tests of the gravity wave and rotor theory, which has in many cases been tested and studied for idealized orography but less for real cases. However, intensive observations campaigns such as the T-REX (Grubišić et al. 2008) have significantly improved the available datasets. However, systematic three-dimensional observations at high temporal resolution would be invaluable. The Monitoring the Atmospheric Boundary Layer in the Artic experiment (MABLA) will address this and is being prepared at Gufuskálar in west Iceland where observations of winds, temperatures, and turbulent fluxes will be made in a 400-m-high mast in a climate with frequent deep extratropical cyclones (Ólafsson et al. 2009).

As often is the case, there was no warning (i.e., SIGMET) issued for this region until after the incident. However, it is evident that this event could have been forecast quite accurately, but not with the NWP tools used at that time in aviation forecasts. Their resolution is not adequate and is typically of the order of 10–30 km or even coarser, although steps are now being taken to develop better weather warning systems based on numerical models at significantly higher resolutions. Previously, Ólafsson and Ágústsson (2009) showed that finescale simulations over complex terrain can successfully predict mountain-wave-induced turbulence near the tropopause level and consequently they may aid in avoiding turbulence incidents at the international flight levels. This event underscores the urgency of delivering such high-resolution products to pilots, for aviation needs in the lower troposphere where atmospheric turbulence may be the most intense and the most hazardous to aviation.

Acknowledgments. This study is a result of a long-lasting collaboration with the airlines operating in Iceland and their pilots. We thank the pilots of Ernir Air for the collaboration in the data collection. The study was supported by the Kvískerjasjóður fund, and it is carried out in connection with the RÁV project, which is supported by the Icelandic research fund (RANNÍS). We acknowledge the anonymous reviewers for their constructive comments.

REFERENCES

Ágústsson, H., and H. Ólafsson, 2004: Mean gust factors in complex terrain. *Meteor. Z.,* **13** (2), 149–155.

——, and ——, 2007: Simulating a severe windstorm in complex terrain. *Meteor. Z.,* **16** (1), 111–122.

——, and ——, 2010: The bimodal downslope windstorms at Kvísker. *Meteor. Atmos. Phys.,* **116,** 27–42, doi:10.1007/s00703-010-0075-y.

Bao, J.-W., S. A. Michelson, L. Kantha, and J. W. Brown, 2008: Implementation of a two-equation vertical turbulent mixing scheme in a mesoscale atmospheric model. NOAA Tech. Memo. OAR PSD-311, National Oceanic and Atmospheric Administration, 33 pp.

Deng, A., and D. R. Stauffer, 2006: On improving 4-km mesoscale model simulations. *J. Appl. Meteor. Climatol.,* **45,** 361–381.

Doyle, J. D., and D. R. Durran, 2002: The dynamics of mountain-wave induced rotors. *J. Atmos. Sci.,* **59,** 186–201.

——, and ——, 2004: Recent developments in the theory of atmospheric rotors. *Bull. Amer. Meteor. Soc.,* **85,** 337–342.

——, and ——, 2007: Rotor and subrotor dynamics in the lee of three-dimensional terrain. *J. Atmos. Sci.,* **64,** 4202–4221.

——, M. A. Shapiro, Q. Jiang, and D. L. Bartels, 2005: Large-amplitude mountain wave breaking over Greenland. *J. Atmos. Sci.,* **62,** 3106–3126.

——, V. Grubišić, W. O. J. Brown, S. F. J. D. Wekker, A. Dörnbrack, Q. Jiang, S. D. Mayor, and M. Weissmann, 2009: Observations and numerical simulations of subrotor vortices during T-REX. *J. Atmos. Sci.,* **66,** 1229–1249.

——, and Coauthors, 2011: An intercomparison of T-REX mountain-wave simulations and implications for mesoscale predictability. *Mon. Wea. Rev.,* **139,** 2811–2831.

Durran, D. R., 1990: Mountain waves and downslope winds. *Atmospheric Processes over Complex Terrain, Meteor. Monogr.,* No. 45, Amer. Meteor. Soc., 59–81.

——, 2003: Mountain waves and downslope winds. *Encyclopedia of Atmospheric Sciences,* J. R. Holton, J. Pyle, and J. A. Curry, Eds., Elsevier Science Ltd., 1161–1169.

Feltz, W. F., K. M. Bedka, J. A. Otkin, T. Greenwald, and S. A. Ackerman, 2009: Understanding satellite-observed mountain-wave signatures using high-resolution numerical model data. *Wea. Forecasting,* **24,** 76–86.

Gohm, A., G. J. Mayr, A. Fix, and A. Giez, 2008: On the onset of bora and the formation of rotors and jumps near a mountain gap. *Quart. J. Roy. Meteor. Soc.,* **134** (630), 21–46.

Grell, G. A., J. Dudhia, and D. R. Stauffer, 1994: A description of the fifth-generation Penn State/NCAR Mesoscale Model (MM5). Tech. Rep. NCAR/TN-398+STR, National Center for Atmospheric Research, 122 pp.

Grubišić, V., and J. M. Lewis, 2004: Sierra wave project revisited: 50 years later. *Bull. Amer. Meteor. Soc.,* **85,** 1127–1142.

——, and B. J. Billings, 2007: The intense lee-wave rotor event of Sierra rotors IOP 8. *J. Atmos. Sci.,* **64,** 4178–4201.

——, and M. Orlić, 2007: Early observations of rotor clouds by Andrija Mohorovičić. *Bull. Amer. Meteor. Soc.,* **88,** 693–700.

——, and I. Stiperski, 2009: Lee-wave resonances over double bell-shaped obstacle. *J. Atmos. Sci.,* **66,** 1205–1228.

——, and Coauthors, 2008: The terrain-induced rotor experiment: A field campaign overview including observational highlights. *Bull. Amer. Meteor. Soc.,* **89,** 1513–1533.

Hertenstein, R. F., and J. P. Kuettner, 2005: Rotor types associated with steep lee topography: Influence of the wind profile. *Tellus,* **57A,** 117–135.

Horvath, K., D. Koracin, R. Vellore, J. Jiang, and R. Belu, 2012: Sub-kilometer dynamical downscaling of near-surface winds in complex terrain using WRF and MM5 mesoscale models. *J. Geophys. Res.,* **117,** D11111, doi:10.1029/2012JD017432.

Janjić, Z. I., 1994: The step-mountain eta coordinate model: Further development of the convection, viscous sublayer, and turbulent closure schemes. *Mon. Wea. Rev.,* **122,** 927–945.

——, 2001: Nonsingular implementation of the Mellor–Yamada level 2. 5 scheme in the NCEP Meso model. Scientific Rep. Office Note 437, National Centers for Environmental Prediction, 61 pp.

Jiang, Q., J. D. Doyle, and R. B. Smith, 2006: Interaction between trapped waves and boundary layers. *J. Atmos. Sci.,* **63,** 617–633.

Küttner, J. P., 1938: Moazagotl und föhnwelle. *Beitr. Phys. Atmos.,* **25,** 79–114.

Lane, T. P., J. Doyle, R. Sharman, M. A. Shapiro, and C. Watson, 2009: Statistics and dynamics of aircraft encounters of turbulence over Greenland. *Mon. Wea. Rev.,* **137,** 2687–2702.

Lilly, D. K., 1978: A severe downslope windstorm and aircraft turbulence event induced by a mountain wave. *J. Atmos. Sci.,* **35,** 59–77.

Mellor, G. L., and T. Yamada, 1982: Development of a turbulence closure model for geophysical fluid problems. *Rev. Geophys. Space Phys.,* **20,** 851–875.

Nance, L. B., and D. R. Durran, 1997: A modeling study of nonstationary trapped mountain lee waves. Part I: Mean flow variability. *J. Atmos. Sci.,* **54,** 2275–2291.

——, and ——, 1998: A modeling study of nonstationary trapped mountain lee waves. Part II: Nonlinearity. *J. Atmos. Sci.,* **55,** 1429–1445.

Ólafsson, H., and H. Ágústsson, 2007: The Freysnes downslope windstorm. *Meteor. Z.,* **16** (1), 123–130.

——, and ——, 2009: Gravity wave breaking in easterly flow over Greenland and associated low level barrier- and reverse tip-jets. *Meteor. Atmos. Phys.,* **104** (3), 191–197.

——, N. Jónasson, and S. Karlsdóttir, 2006: Háupplausnarreikningar til almennrar spágerðar (HRAS), lokaskýrsla (high-resolution atmospheric simulations, final report). Tech. Rep. 06011, Veðurstofa Íslands, 26 pp. [Available online at http://www.vedur.is/um-vi/utgafa/greinargerdir/.]

——, Ó. Rögnvaldsson, J. Reuder, H. Ágústsson, G. N. Petersen, H. Björnsson, T. Jónsson, and J. E. Kristjánsson, 2009: Monitoring the Atmospheric Boundary Layer in the Artic (MABLA): The Gufuskálar project. *Proc. 30th Int. Conf. on Alpine Meteorology (ICAM),* Rastatt, Germany, Deutscher Wetterdienst, Annalen der Meteorologien 44, 192–193. [Available online at http://www.pa.op.dlr.de/icam2009/extabs/.]

Reinecke, P. A., and D. R. Durran, 2009: Initial condition sensitivities and the predictability of downslope winds. *J. Atmos. Sci.,* **66,** 3401–3418.

Renfrew, I. A., and Coauthors, 2008: The Greenland Flow Distortion Experiment. *Bull. Amer. Meteor. Soc.,* **89,** 1307–1324.

Rögnvaldsson, Ó., J.-W. Bao, and H. Ólafsson, 2007: Sensitivity simulations of orographic precipitation with MM5 and comparison with observations in Iceland during the Reykjanes Experiment. *Meteor. Z.,* **16** (1), 87–98.

——, H. Ágústsson, and H. Ólafsson, 2011a: Aflræn niðurkvörðun veðurs innan LOKS verkefnisin (Dynamical downscaling of weather within the LOKS-project). Tech. Rep., Reiknistofa í veðurfræði, 29 pp. [Available online at http://riv.is/pages/1287-greinar-og-skyrslur/.]

——, J.-W. Bao, H. Ágústsson, and H. Ólafsson, 2011b: Downslope windstorm in Iceland–WRF/MM5 model comparison. *Atmos. Chem. Phys.,* **11** (1), 103–120, doi:10.5194/acp-11-103-2011.

Scorer, R. S., 1949: Theory of waves in the lee of mountains. *Quart. J. Roy. Meteor. Soc.,* **75** (323), 41–56.

Sheridan, P., and S. Vosper, 2012: High-resolution simulations of lee waves and downslope winds over the Sierra Nevada during T-REX IOP 6. *J. Appl. Meteor. Climatol.,* **51,** 1333–1352.

Skamarock, W. C., and Coauthors, 2008: A description of the Advanced Research WRF version 3. Tech. Rep. NCAR/TN-475+STR, National Center for Atmospheric Research, 125 pp.

Smith, R. B., 1980: Linear theory of stratified flow past an isolated mountain. *Tellus,* **32,** 348–364.

——, 1987: Aerial observations of the Yugoslavian Bora. *J. Atmos. Sci.,* **44,** 269–297.

Smith, C. M., and E. D. Skyllingstad, 2009: Investigation of upstream boundary layer influence on mountain wave breaking and lee wave rotors using a large eddy simulation. *J. Atmos. Sci.,* **66,** 3147–3164.

——, and ——, 2011: Effect of inversion height and surface heat flux on downslope windstorms. *Mon. Wea. Rev.,* **139,** 3750–3764.

Smith, R. B., Q. Jiang, and J. D. Doyle, 2006: A theory of gravity wave absorption by a boundary layer. *J. Atmos. Sci.,* **63,** 774–781.

Stiperski, I., and V. Grubišić, 2011: Trapped lee wave interference in the presence of surface friction. *J. Atmos. Sci.,* **68,** 918–936.

Teixeira, M. A. C., J. L. Argain, and P. M. A. Miranda, 2013: Drag produced by trapped lee waves and propagating mountain waves in a two-layer atmosphere. *Quart. J. Roy. Meteor. Soc.,* **139B,** 964–981.

Valkonen, T., T. Vihma, S. Kirkwood, and M. M. Johansson, 2010: Fine-scale model simulation of gravity waves generated by Basen Nunatak in Antarctica. *Tellus,* **62A,** 319–332.

Vosper, S. B., 2004: Inversion effects of mountain lee waves. *Quart. J. Roy. Meteor. Soc.,* **130,** 1723–1748.

Wyngaard, J. C., 2004: Toward numerical modeling in the ''terra incognita.'' *J. Atmos. Sci.,* **61,** 1816–1826.